MICROWAVE TUNABLE LASER SOURCE: A STABLE, PRECISION TUNABLE HETERODYNE LOCAL OSCILLATOR

Glen W. Sachse
NASA Langley Research Center

SUMMARY

A tunable laser source utilizing a wideband electro-optic modulator and a CO_2 laser has been developed. Its precision tunability and high stability are demonstrated with examples of laboratory spectroscopy. Heterodyne measurements are also presented to demonstrate the performance of the laser source as a heterodyne local oscillator.

INTRODUCTION

A stable, precision-tunable laser source for the intermediate infrared (IR) would have numerous applications including: remote sensing of the earth, planetary, and stellar atmospheres, injection locking of high-pressure laser amplifiers, ultra-high resolution spectroscopy, isotope separation, etc. Diode lasers possess wide tunability in this region and have found wide usage in laboratory spectroscopy. However, operational difficulties primarily associated with cryogenic requirements and lack of built-in wavelength information have hampered the application of diode lasers outside the laboratory. Although several heterodyne measurements using the diode laser have been reported (refs. 1 to 3), mode competition problems (ref. 4) present additional difficulties in their use as heterodyne local oscillators. On the other hand, several line-tunable gas lasers, including the CO_2, CO, and N_2O lasers, also exist in the intermediate IR. These lasers generally possess high-frequency stability and accuracy, possess good mode quality, and operate at or near room temperature. The CO_2 laser and, to a limited extent, the CO laser have been used successfully as heterodyne local oscillators in several instruments. (See refs. 5 to 7.) However, their discrete tunability restricts their use to chance coincidences with frequencies of interest (i.e., specific absorption-line or window frequencies).

An alternative approach for providing tunability in the intermediate infrared is to utilize wideband electro-optic modulators to generate tunable optical sidebands on gas-laser carriers. This approach has the potential for providing some of the attractive features of gas lasers along with piecewise continuous tunability over significant portions of the infrared where line-tunable gas lasers of moderate power output ($\geq$ 1 W) exist. Absolute wavelength accuracy and stability of such a laser source is limited only by the gas laser. Its room-temperature operating capability may also make it more readily applicable to in-the-field operation.

Several infrared modulators (refs. 8 to 10) have been developed; however, only the GaAs waveguide modulator (ref. 11) developed by Peter Cheo of United

Technologies Research Center is discussed in this paper. The Microwave Tunable Laser Source (MTLS) is an optical/microwave system which was developed utilizing the GaAs modulator (ref. 12). In this paper the MTLS is briefly described and examples of laboratory spectroscopy and a characterization of its heterodyne properties are presented.

MTLS DESCRIPTION

The key component of the MTLS is the GaAs waveguide modulator. The modulator utilizes the linear electro-optic effect (ref. 13) to generate optical sidebands on an incident CO_2 laser carrier. The sidebands are located at the sum and difference frequencies and may be tuned by simply varying the microwave frequency within the modulator bandpass. The modulator was originally reported to have a nominal 3-dB bandpass of 5 GHz. (See ref. 11.) Since then the sideband tunability of this same modulator has been improved to $\approx$ 10 GHz. (See ref. 12.) This bandpass (see fig. 1) is located between the offset frequencies of 8 and 18 GHz. The conversion efficiency (ratio of output sideband to carrier power) reaches a maximum at 10 GHz, where it equals 0.7 percent for 20 watts of microwave power. The optical throughput of the modulator is 20 percent, and the output beam is a slowly diverging ellipse with a major to minor axis ratio of 3. After more than a year of use in our laboratory, no significant changes in the modulator performance have been observed.

The MTLS transforms the multifrequency output of the modulator into a precisely tunable monochromatic output. The carrier, which is typically 150 to 300 times more intense than either sideband, is suppressed by passing the modulator output through a heated ($\approx$ 60°C), 0.375-m long white cell with an internal 22-m path and containing low-pressure CO_2. Figure 2 contains Fabry-Perot scans of the white-cell output which indicate that, with the aforementioned white-cell parameters, the carrier is suppressed to a level equal to or less than the sidebands for the lasing transitions P(10) to P(30). Single-frequency operation is achieved by dither stabilizing a tunable Fabry-Perot etalon on the desired sideband, thereby rejecting the remaining carrier and extra sideband. A small desk-top calculator presently controls the microwave sweeper, power meter, and frequency counter. The controller can accurately place the microwave frequency anywhere between 8 and 18 GHz, or can perform high-precision scans with microwave frequency resolution well below 0.1 MHz. For a perspective of the optical and microwave powers involved, the single frequency MTLS output is typically 0.5 mW for an incident CO_2 laser power of 3 W and 20 W of microwave power. At least a 50-percent improvement in MTLS output is realizable through straightforward increases in the system optical throughput.

By utilizing the line tunability of CO_2 lasers, significant spectral coverage over the 9- to 12-μm region is achievable. Since the average CO_2 line separation is about 50 GHz, approximately 40-percent spectral coverage is achieved within the lasing region of a single CO_2 isotope laser. Figure 3 shows the calculated MTLS spectral coverage that results with five different CO_2 isotope lasers ($C^{12}O_2^{16}$, $C^{12}O_2^{18}$, $C^{13}O_2^{16}$, $C^{13}O_2^{18}$, and $C^{14}O_2^{16}$). This bar graph was generated by dividing the 9- to 12-μm region into bins each 2 cm^{-1}

(60 GHz) wide and calculating the percentage spectral coverage within each bin. Laser tunability was assumed to be P(10) to P(30) and R(10) to R(30) in each band. The calculations indicate that the spectral coverage approaches 100 percent in regions of high isotope overlap, and exceeds 50 percent when averaged across the entire 9- to 12-μm region. The N_2O laser tunability should add significantly to the spectral coverage, particularly in the 10- to 11-μm region. However, its tunability was not included in the preceding calculation.

SPECTROSCOPIC MEASUREMENTS

To illustrate the precision tunability of the system, laboratory spectroscopy of SF_6 and NH_3 was performed. The $C^{12}O_2^{16}$ laser used in these measurements was not grating-tunable; consequently, laser operation was confined to a few lines in the 10.6-μm band. The single-frequency sideband output was digitally stepped in intervals of 0.6 MHz by command from the calculator. A scan rate of 6 MHz/sec was used in these measurements. A beam splitter diverted approximately 50 percent of the optical beam to a pyroelectric detector, which served to monitor power changes during the frequency sweep. The remaining optical power passed through the 12.5-cm-long sample cell and was focused on a second pyroelectric detector. The two detector outputs were analog ratioed to provide the normalized spectra shown in figures 4 and 5.

In figure 4(a), the upper sideband of the P(20) line was stepped 10 000 times between 12 and 18 GHz, which revealed the complicated absorption spectrum of low-pressure SF_6. In figure 4(b), the same sideband was scanned across a narrower frequency interval to illustrate that the narrow 38-MHz FWHM absorption lines are easily resolved by the MTLS. In figure 5, the MTLS was scanned across two NH_3 lines - one located within the tuning range of the lower sideband, and the other within the range of the upper sideband of the P(18) CO_2 line. The determination of the line positions differed significantly from Taylor (ref. 14), but agreed to within 250 MHz with the positions reported by Curtis (ref. 15). When these measurements were performed, the microwave counter, which provides frequency accuracy to better than 1 kHz, was not in use and the CO_2 laser was not actively stabilized. The frequency accuracy of the sweep oscillator, independent of the frequency counter, is specified by the manufacturer as ±20 MHz, and the stability of the CO_2 laser during the measurement period was estimated to be better than ±5 MHz. Through stabilization of the CO_2 laser, spectroscopic measurements with frequency resolution better than 1 MHz (0.000033 cm^{-1}) should be readily achievable.

HETERODYNE CHARACTERIZATION

Before heterodyne measurements were performed, the noise characteristics of the sidebands between 0.1 and 100 MHz were investigated. This frequency range corresponded to the approximate bandpass of the heterodyne photomixer, IF amplifier, and filter. A qualitative look at the integrated noise within this bandpass was accomplished by monitoring the rectified RF photomixer output while the Fabry-Perot was spectrally scanned across the carrier and sidebands. The upper right photograph in figure 6 shows that sizable rectified noise is present at the sideband frequencies but is barely discernible at the carrier

frequency. For this particular measurement, the carrier and sideband power levels were equal as shown by the Fabry-Perot scan of the quasi-dc photomixer output (upper left photograph). The carrier power was made to equal the sideband power by fine tuning the white-cell temperature. It was found that the sideband noise was a function of the traveling-wave-tube (TWT) amplifier drive power and that a dip in the noise was achieved by operating the amplifier beyond the saturation point at a microwave output power of 15.6 W. (The output power at the saturation point was about 20 W.) Interestingly, as the drive was decreased, the sideband noise grew rapidly and reached a maximum when the microwave output was 7.2 W, which is below saturation. The dc sideband power (lower left photograph) responded proportionally to the microwave power as expected, but the noise peaks (lower right photograph) increased approximately 12 dB. Since the RF detector output was proportional to the product of the dc sideband power and the sideband noise power, the actual increase in sideband noise was approximately 15 dB. Further reduction of the drive power resulted in the noise peaks decreasing at the same rate, which implied a constant sideband noise power. The oscilloscope scale was the same for each photograph. The quasi-dc photomixer output was not preamplified; however, the RF output was amplified 60 dB.

The interpretation of these data is as follows: The broadband noise output P_N of an amplifier consists of amplified Johnson noise and internally generated noise. These noise contributions are independent of the drive power, provided the amplifier is operating in the linear region. For a matched input,

$$P_N = kTGN$$

where k is Boltzmann's constant, T is room temperature, G is the TWT gain, and N is the noise factor. The noise figure (the dB equivalent of the noise factor) is the measure of the internally generated noise and was manufactured specified to be 35 dB. The small signal gain was measured to be 62 dB at the operating frequency. Since the sweep oscillator is capable of delivering 10 dBm, only 33-dB TWT gain is necessary to reach the desired 20 watts microwave output. Because the drive signal was by necessity strongly attenuated, this excess TWT gain in effect contributed nearly the same signal-to-noise (S/N) degradation as did the noise figure when the TWT was operated in the small signal region. The large reduction in sideband noise observed when the TWT was operated well into saturation was simply due to a 15-dB gain compression which reduced P_N according to the preceding equation.

The properties of the sideband noise were further analyzed by monitoring the photomixer amplifier output with a spectrum analyzer. Three conditions of photomixer illumination were investigated. In the bottom spectrum of figure 7(a), the photomixer was not illuminated, which resulted in a noise spectrum associated with the photomixer and the IF amplifier. Next, the etalon bandpass was tuned so that only the carrier illuminated the photomixer. This resulted in a broadband noise increase of $\approx$ 3 dB associated with the carrier shot noise. When the etalon was tuned to the sideband frequency, the expected large increase in noise was observed. The increase above the carrier noise amounted to $\simeq$ 16 dB at the low-frequency end and $\approx$ 12 dB near 100 MHz. The sideband and carrier power were roughly equal at 140 μW, and the TWT was operated well into saturation to yield the minimum sideband noise.

With the TWT used in the aforementioned measurements, the minimum sideband noise was achieved with the TWT gain compressed to 47 dB and an output power of 15.6 W. Under these conditions, the drive signal had to be attenuated ≈ 15 dB, which resulted in a corresponding microwave S/N degradation. Since the sideband noise was 12 to 16 dB greater than the carrier shot noise, a lower-gain TWT amplifier not requiring attenuation of the input drive signal might be expected to introduce a noise level comparable to the shot noise. A lower-power (10 W) TWT amplifier with low gain and a manufacturer-specified noise figure of 35 dB was located and its noise spectral characteristics were investigated in figure 7(b). With no input attenuation, the amplifier was driven to 9.6 W output. The carrier power was again made to equal sideband power. At a reduced carrier power of 100 μW, a shot noise of 1.5 to 2 dB above the "photomixer" noise was observed. As expected, the broadband component of the sideband noise decreased sharply to a level 3 to 4.5 dB above the shot noise. Narrow-band noise at 5 and 15 MHz is probably due to coherent oscillations (ref. 16) in the traveling wave tube, and is not generally found in a well-designed tube that is operating properly. Further reductions in the sideband noise can be achieved by lowering the noise figure. Low-gain TWT amplifiers are commercially available with noise figures on the order of 30 dB. An alternative method of lowering the overall noise figure would be to include an intermediate amplifier of low noise figure.

A heterodyne measurement of the thermal radiation from a 1273 K blackbody was performed to compare the S/N achieved using the carrier and the sideband as local oscillators. The collimated blackbody beam was passed through a long-wave pass filter (8.9 μm cut-on wavelength) in order to minimize the contribution of the chopped thermal shot noise to the heterodyne IF output. A 50-percent beam splitter was used to bring the local oscillator and blackbody beams into coincidence. During the experiment the MTLS delivered 220 μW after the beamsplitter, but generated a detector photo-current the equivalent of only 100 μW. The excessive detector overfill occurred since no attempt was made to optically match the elliptical modulator output with the circular detector. A 10-MHz high-pass filter was added to the heterodyne IF stage in order to reject the strong TWT-generated noise peak at 5 MHz. Thus, the total heterodyne bandpass was 90 MHz.

The results of the heterodyne measurements are shown in figure 8. The rectified outputs of the heterodyne IF state are plotted against time for three local oscillator cases - carrier, no local oscillator, and sideband. In each case a measurement period of 30 sec is plotted. The RC time constant of the lock-in amplifier filter was 1.25 sec, which is equivalent to an effective bandpass of 0.1 Hz for a 12 dB/octave filter. As expected, the heterodyne signal magnitudes were very nearly equal and the sideband local oscillator exhibited somewhat poorer S/N than the carrier. The non-zero output registered with no local oscillator was due to the chopped thermal shot noise.

CONCLUDING REMARKS

A stable precision tunable laser source has been developed using a wide-band electro-optic modulator and a CO_2 laser. With the use of five CO_2 isotope

lasers and the 8 to 18 GHz sideband offset tunability of the modulator, calculations indicate that > 50 percent spectral coverage in the 9- to 12-μm region is achievable. This wavelength region is especially important for the development of optical atmospheric sensing instrumentation, since it coincides with an atmospheric window and a region where high technology infrared components exist. The wavelength accuracy and stability of this laser source is limited by the CO_2 laser and is more than adequate for the measurement of narrow Doppler-broadened line profiles. This was demonstrated with the spectroscopic measurements of SF_6. The room-temperature operating capability and the programmability of the MTLS are attractive features for its in-the-field implementation. Although heterodyne measurements indicated some S/N degradation when using the MTLS as a local oscillator, there does not appear to be any fundamental limitation to the heterodyne efficiency of this laser source. Through the use of a lower noise-figure TWT amplifier and optical matching of the MTLS output beam with the photomixer, a substantial increase in the heterodyne S/N is expected.

REFERENCES

1. Harward, C. N.; and Hoell, J. M.: Atmospheric Solar Absorption Measurements in the 9-11 Micron Region Using a Diode Laser Heterodyne Spectrometer. Heterodyne Systems and Technology, NASA CP-2138, 1980. (Paper 16 of this compilation.)

2. Ku, R. T.; and Spears, D. L.: High Sensitivity Infrared Heterodyne Radiometer Using a Tunable Diode Laser Local Oscillator. Optics Letters, Vol. 1, No. 3, Sept. 1977, pp. 84-86.

3. Frerking, M. A.; and Muehlner, D. J.: Infrared Heterodyne Spectroscopy of Atmospheric Ozone. Applied Optics, Vol. 16, No. 3, March 1977, pp. 526-528.

4. Harward, C. N.; and Sidney, B. D.: Excess Noise in $Pb_{1-x}Sn_xSe$ Semiconductor Lasers. Heterodyne Systems and Technology, NASA CP-2138, 1980. (Paper 10 of this compilation.)

5. Hoell, J. M.; Harward, C. N.; and Williams, B. S.: Remote Infrared Heterodyne Radiometer Measurements of Atmospheric Ammonia Profiles. Geophysical Research Letters, Vol. 7, No. 5, May 1980, pp. 313-316.

6. Menzies, R. T.: Remote Measurement of CℓO in the Stratosphere. Geophysical Research Letters, Vol. 6, No. 3, March 1979, pp. 151-154.

7. Menzies, R. T.: Use of CO and CO_2 Lasers to Detect Pollutants in the Atmosphere. Applied Optics, Vol. 10, No. 7, July 1971, pp. 1532-1538.

8. Magerl, G.; and Bonek, E.: Broadband Electronically Tunable Resonant Microwave Modulators for CO_2 Lasers. Applied Physics Letters, Vol. 34, No. 7, April 1, 1979, pp. 452-454.

9. Carter, G. M.; and Haus, H. A.: Optical Single Sideband Generation at 10.6 μm. IEEE Journal of Quantum Electronics, Vol. QE-15, No. 4, April 1979, pp. 217-224.

10. Spears, D. L.; and Strauss, A. J.: CdTe Optical Waveguide Modulators. Revue de Physique Appliquee, Vol. 12, Feb. 1977, pp. 401-404.

11. Cheo, P. K.: Generation and Applications of 16 GHz Tunable Sidebands from a CO_2 Laser. Proceedings of the Third International Conference on Laser Spectroscopy, Jackson Lake, WY, July 4-8, 1977.

12. Sachse, G. W.; and Cheo, P. K.: Microwave Tunable Laser Source for the Infrared. Proceedings of the Conference on Laser and Electro-Optical Systems, San Diego, CA, Feb. 26-28, 1980.

13. Kaminow, I. P.; and Turner, E. H.: Electro-optic Light Modulators. Applied Optics, Vol. 5, No. 10, Oct. 1966, pp. 1612-1628.

14. Taylor, F. W.: Spectral Data for the ν_2 Band of Ammonia with Application to Radiative Transfer in the Atmosphere of Jupiter. Journal of Quantitative Spectroscopy and Radiative Transfer, Vol. 13, No. 1973, pp. 1181-1217.

15. Curtis, J. B.: The Vibration-Rotation Bands of NH_3 in the Region 670 cm^{-1} to 1860 cm^{-1}. Ph.D. Thesis, Ohio State University, 1974.

16. Gittins, J. F.: Power Traveling Wave Tubes. American Elsevier Publishing Company, Inc., New York, 1965.

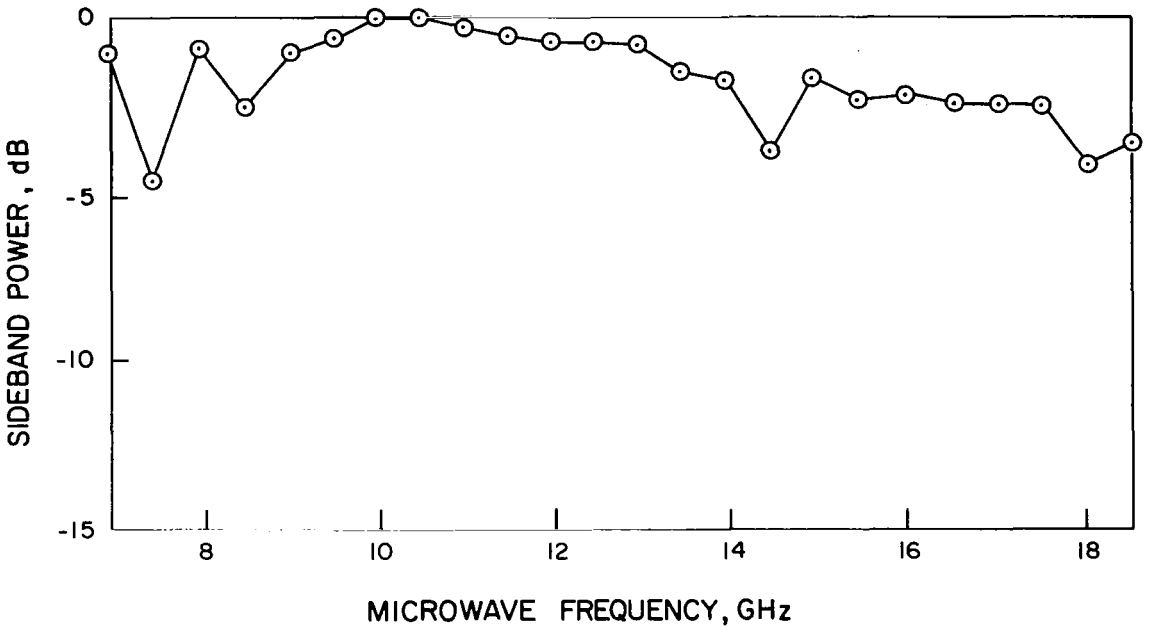

Figure 1.- Microwave bandpass of the GaAs waveguide modulator.

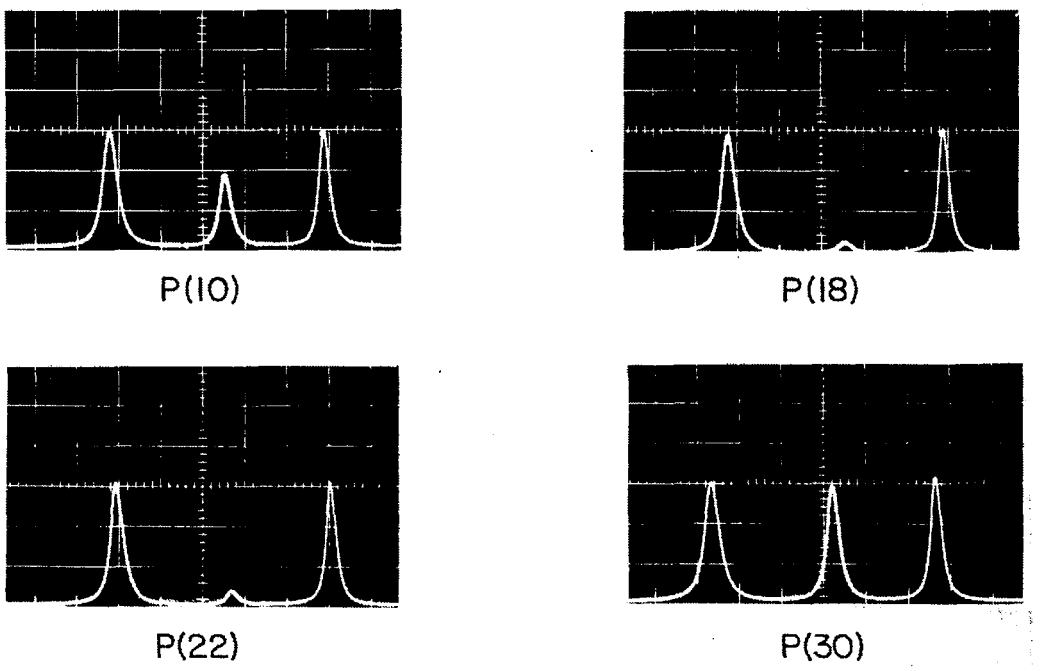

Figure 2.- Fabry-Perot scans of white-cell output as a function of CO_2 laser transition.

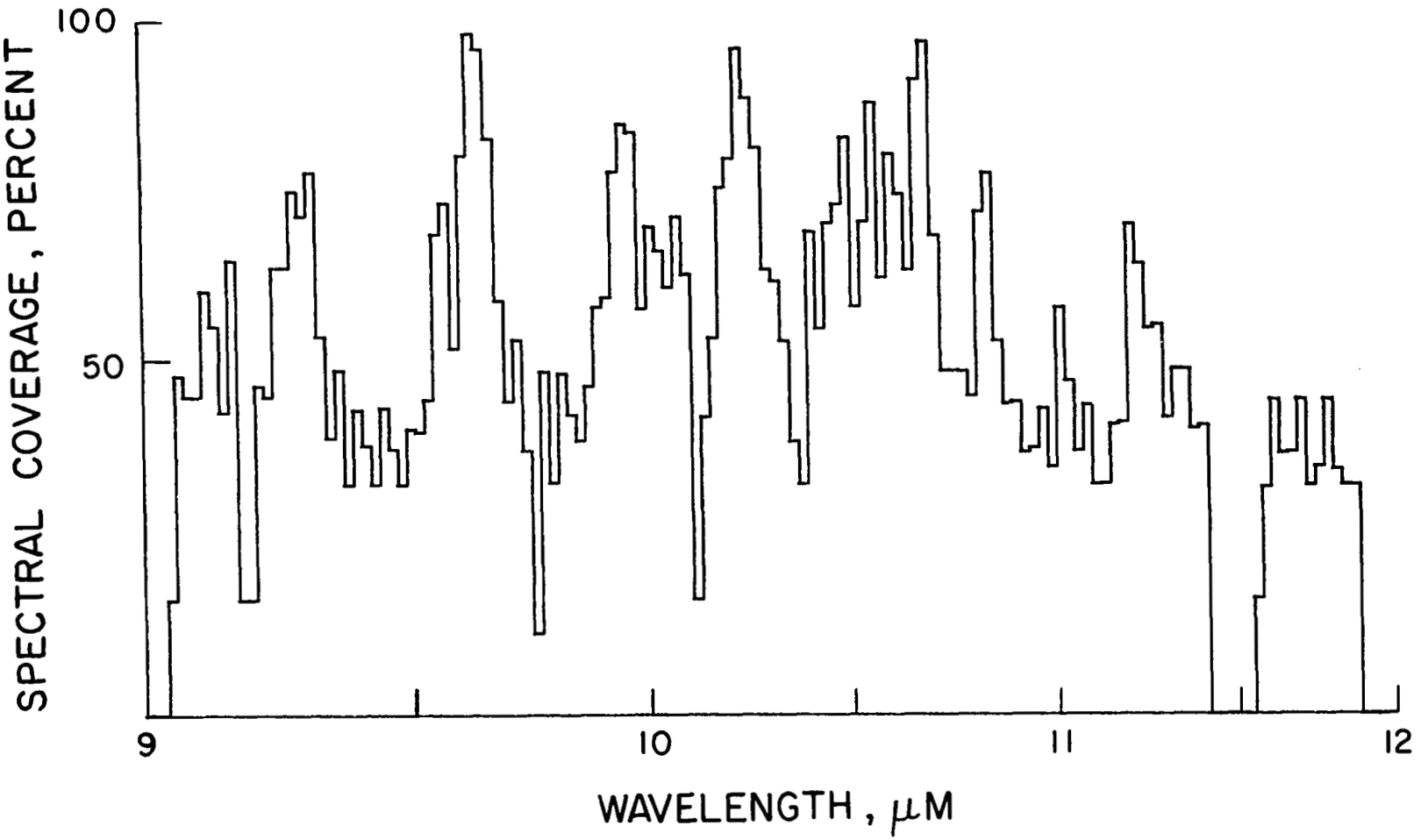

Figure 3.- Calculated spectral coverage of MTLS.

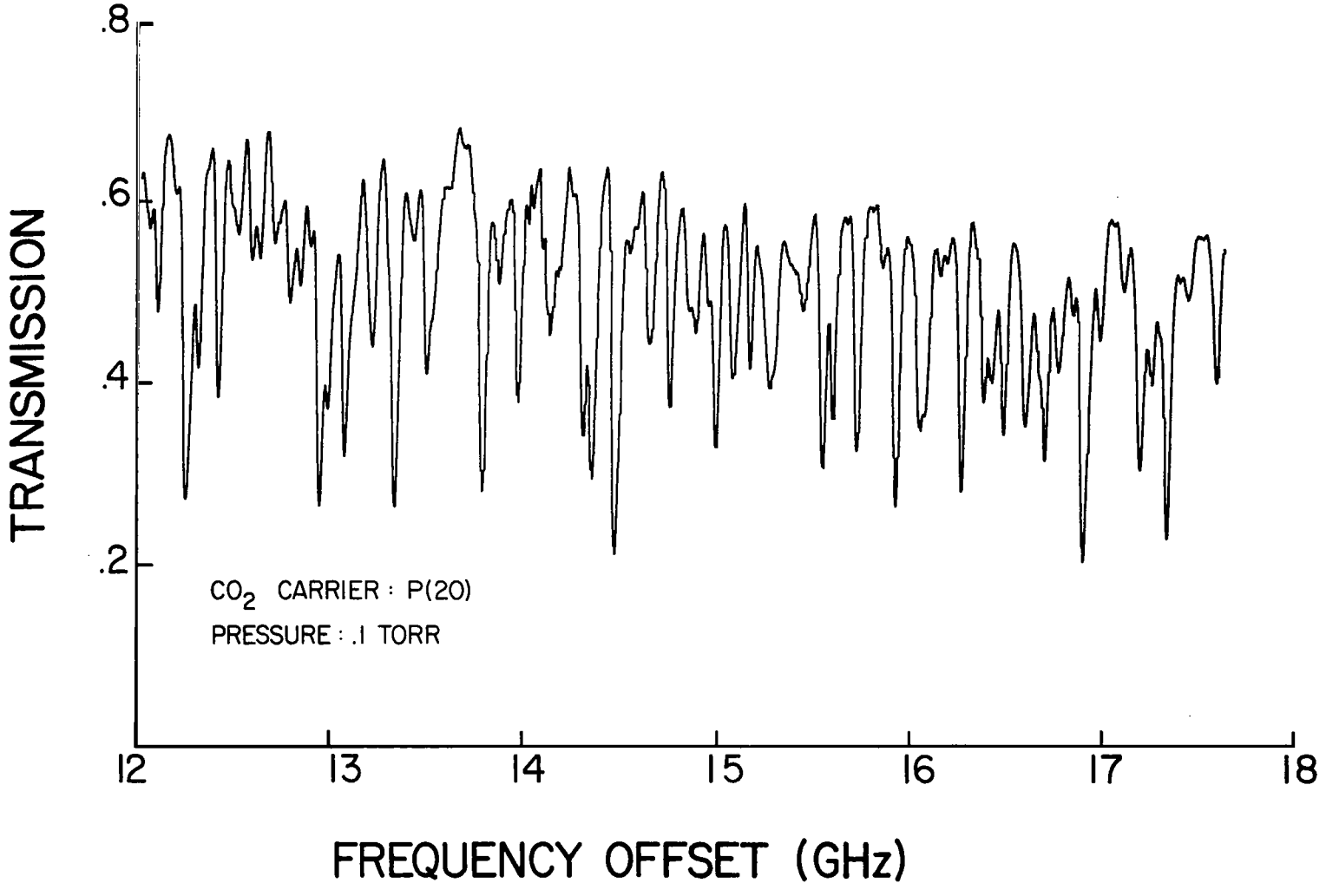

(a) Microwave frequency 12 to 18 GHz.

Figure 4.- SF_6 absorption spectrum resulting from high-resolution scans of upper sideband of P(20) $C^{12}O_2^{16}$ line.

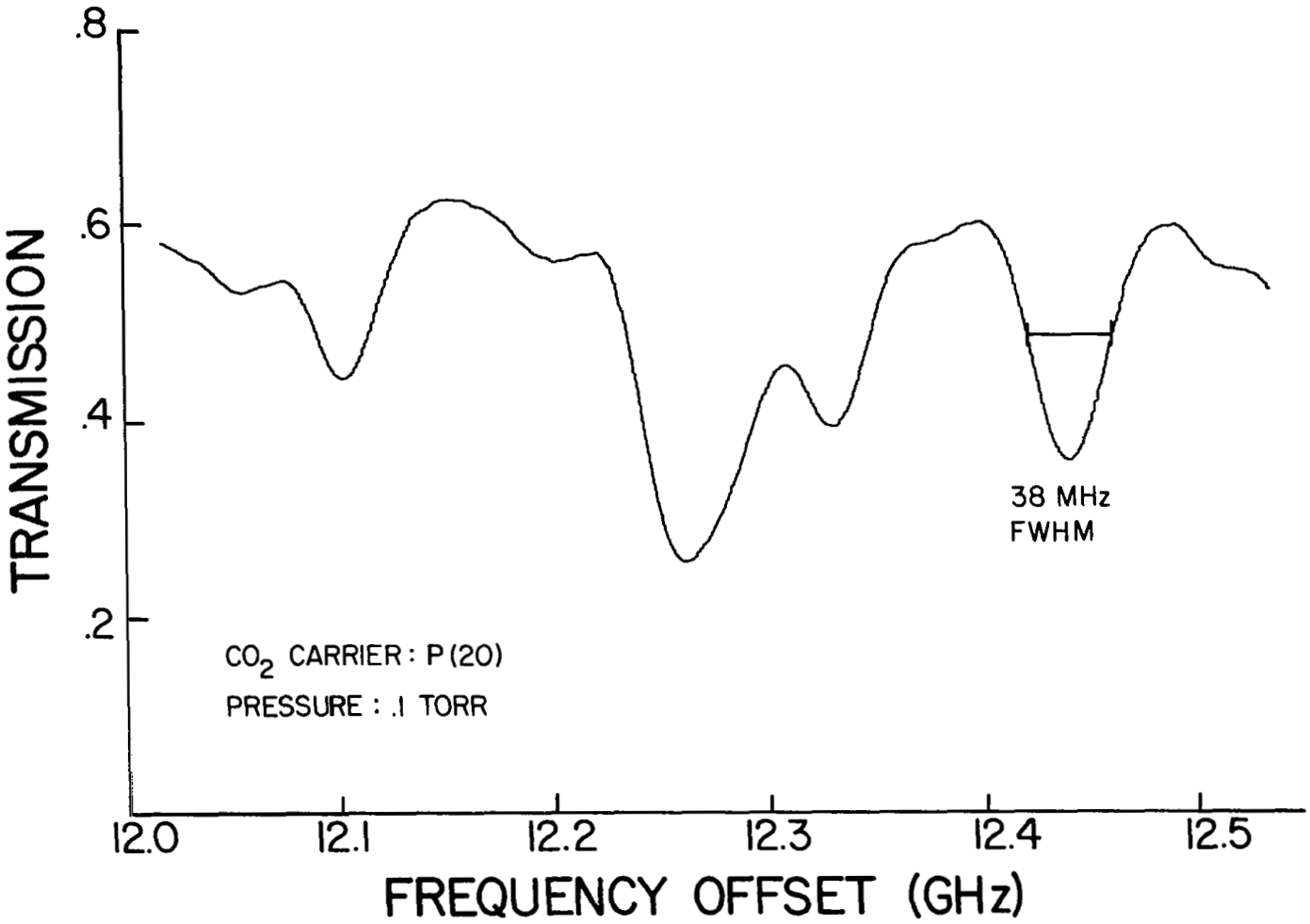

(b) Microwave frequency 12 to 12.5 GHz.

Figure 4.- Concluded.

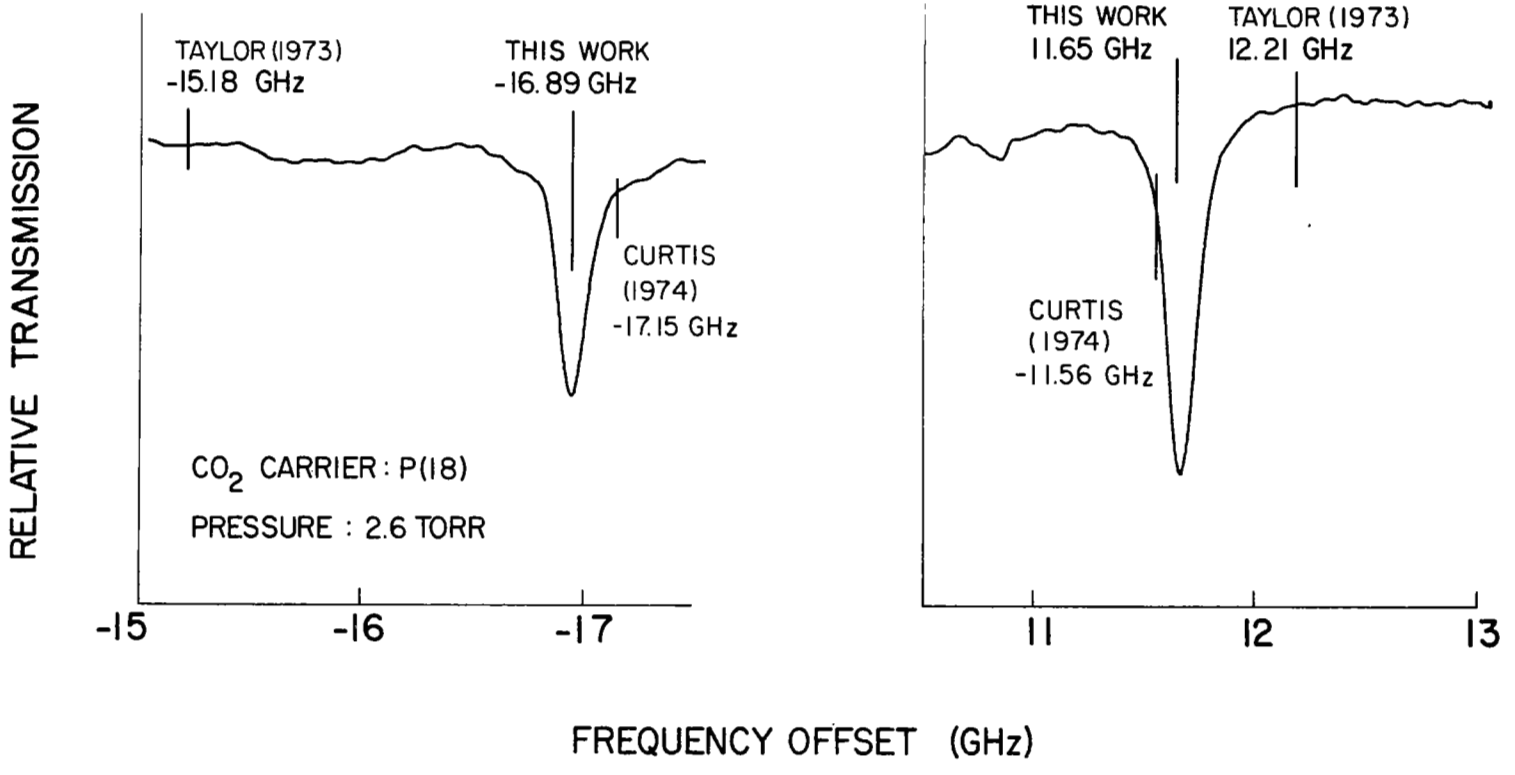

Figure 5.- High-resolution absorption spectra of NH_3.

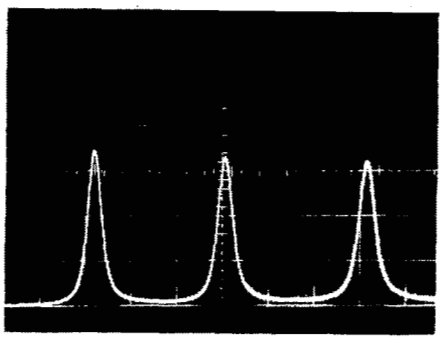

DC PHOTOMIXER OUTPUT
15.5 W MICROWAVE SATURATION

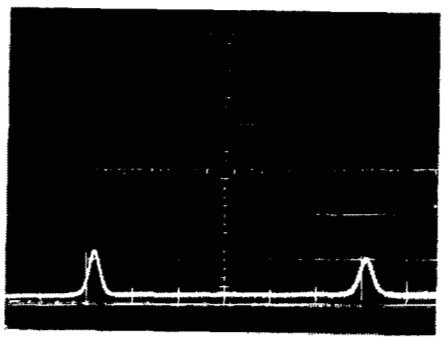

RECTIFIED PHOTOMIXER OUTPUT
100 MHz LOW PASS FILTER
15.5 W MICROWAVE SATURATION

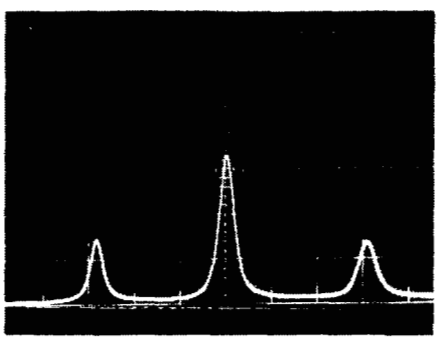

DC PHOTOMIXER OUTPUT
7.2 W MICROWAVE

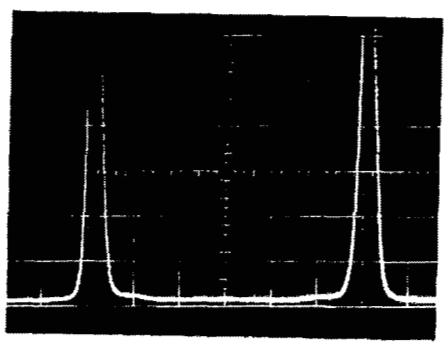

RECTIFIED PHOTOMIXER OUTPUT
100 MHz LOW PASS FILTER
7.2 W MICROWAVE

Figure 6.- Fabry-Perot scans of quasi-dc and rectified RF (100 MHz bandpass) output of photomixer.

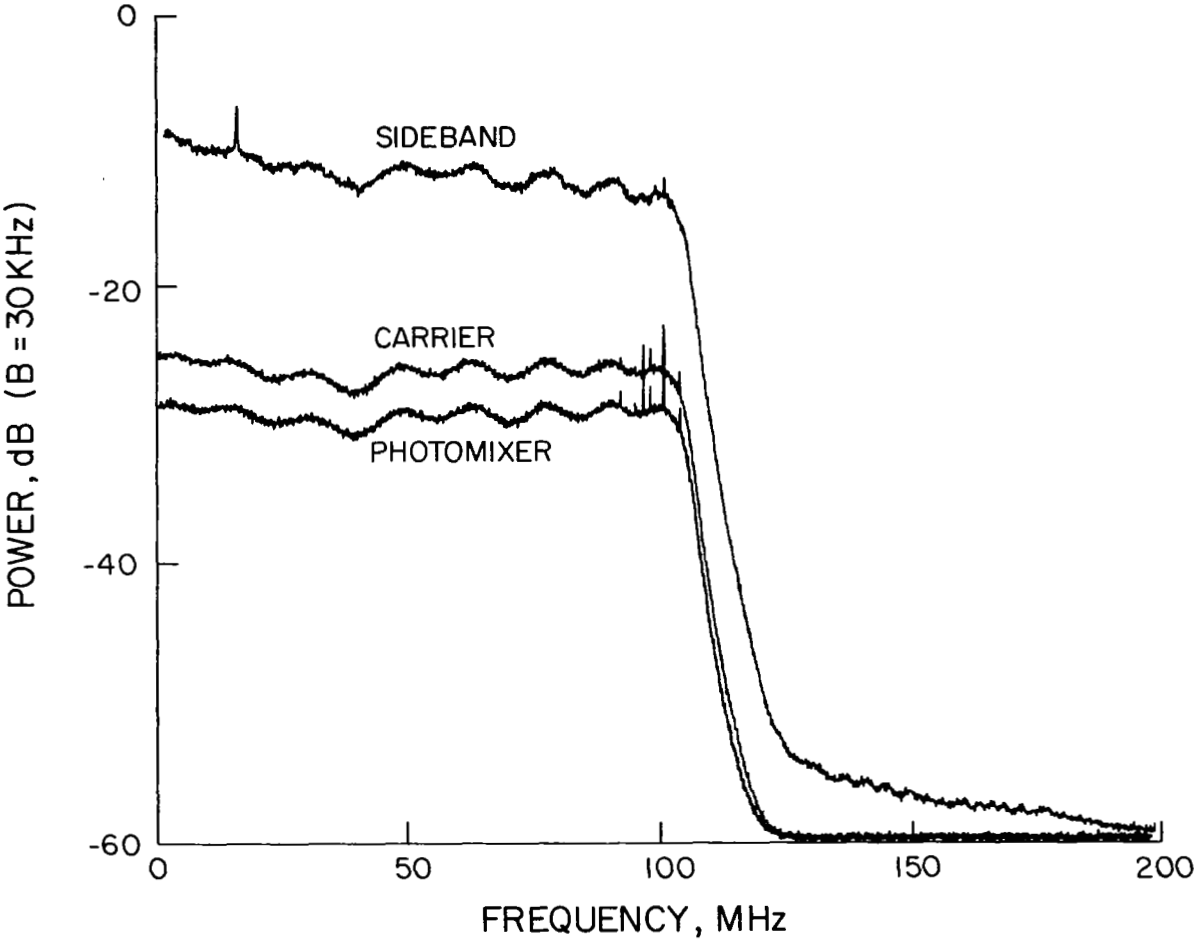

(a) Excess TWT gain introduced substantial noise on optical sideband.

Figure 7.- Spectrum-analyzer displays of photomixer RF output under three conditions of illumination: sideband, carrier, and no illumination.

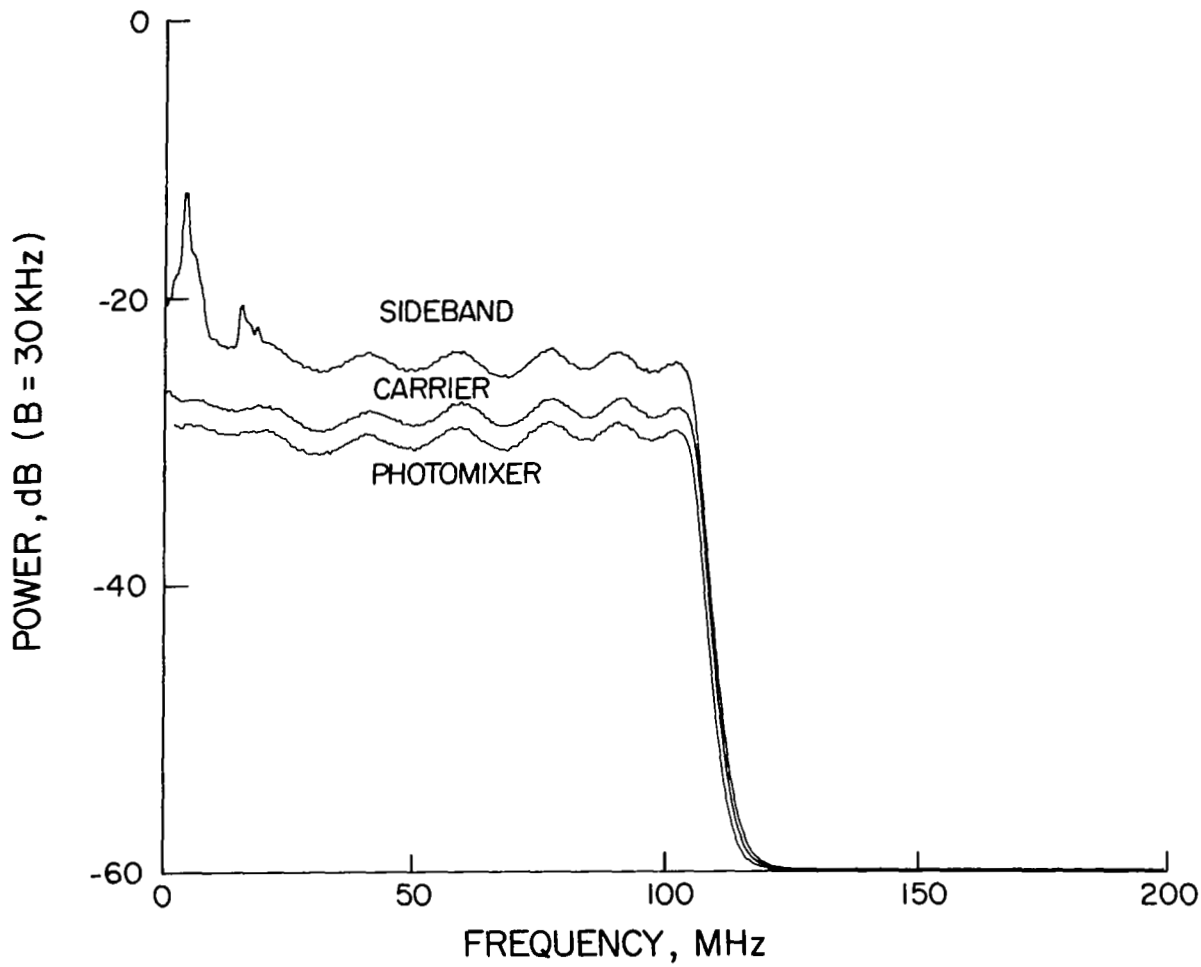

(b) A different TWT exhibiting no excess gain substantially improved the sideband S/N.

Figure 7.- Concluded.

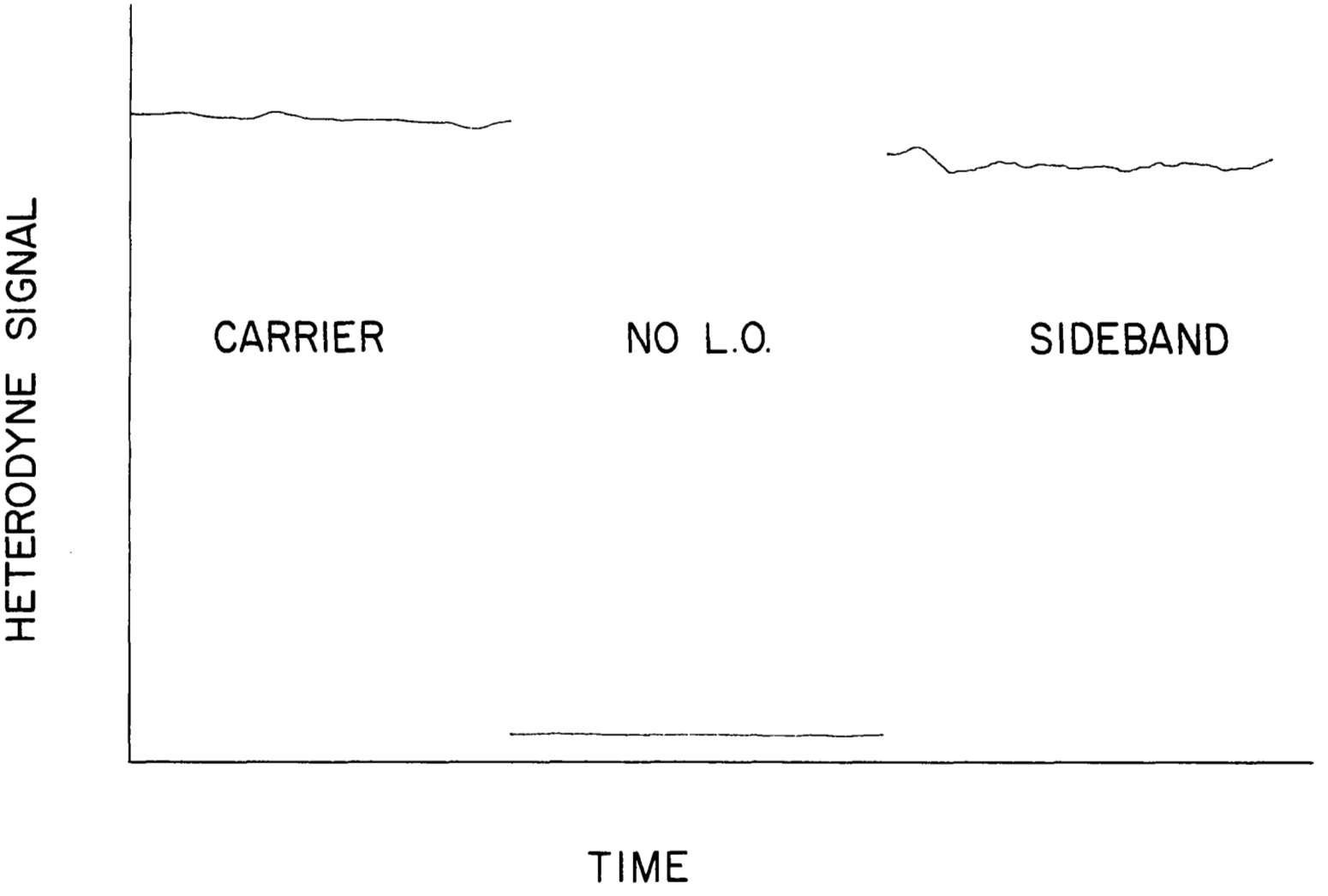

Figure 8.- Heterodyne measurements of a 1273 K blackbody for three cases of local-oscillator illumination: carrier, no local oscillator, and sideband.